Tests with Soft X-rays of an Improved Monolithic SOI Active Pixel Sensor

Syukyo Gando Ryu, Takeshi Go Tsuru, Gregory Prigozhin, Steve Kissel, Marshall Bautz, Beverly LaMarr, Shinya Nakashima, Richard F. Foster, Ayaki Takeda, Yasuo Arai, Toshifumi Imamura, Takafumi Ohmoto, and Atsushi Iwata

***Abstract*—We have been developing monolithic active pixel sensors with 0.2 μm Silicon-On-Insulator (SOI) CMOS technology, called SOIPIX, for high-speed wide-band X-ray imaging spectroscopy on future astronomical satellites. In this work, we investigate a revised chip (XRPIX1b) for soft X-rays used in frontside illumination. The Al Kα line at 1.5 keV is successfully detected and energy resolution of 188 eV (FWHM) is achieved from a single pixel at this energy. The responsivity is improved to 6 μV/electron and the readout noise is 18 electrons rms. Data from 3×3 pixels irradiated with 6.4 keV (Fe Kα) X-rays demonstrates that the circuitry crosstalk between adjacent pixels is less than 0.5%.**

***Index Terms*—active pixel sensor (APS), Silicon-On-Insulator (SOI), CMOS, Multi-point correlated sampling, soft X-ray, frontside illumination, crosstalk, charge splitting.**

I. Introduction

ACTIVE pixel sensors (APSs; [1]–[5]) are being developed as the leading candidate for X-ray imaging spectroscopy in future astronomical satellite missions. At the moment, X-ray charge-coupled devices (CCDs; [6]–[8]) are the standard in the field. However, APSs have many advantages over CCDs, such as direct access to a given pixel, faster readout, higher count rate capability, better radiation hardness, and lower power consumption. APSs for commercial imaging applications have experienced explosive growth in recent years. Substantial progress also has been made for X-ray APSs. For instance, some authors reported that they achieved responsivity above 3 μV/electron [4][5], readout noise below 10 electrons [2][3], and depletion depth above 100 microns [5][9]. On the other hand, unlike X-ray CCDs, APSs are usually subject to issues such as crosstalk and gain non-uniformity. These effects, which are especially important for devices at soft X-rays below 2 keV, have not previously been evaluated for APSs.

With the goal of creating a high-speed wide-band X-ray imaging sensor with spectroscopic capabilities that can replace CCDs, we are developing a novel monolithic APS using the Silicon-on-Insulator (SOI) CMOS technology, i.e., SOIPIX [10][11]. In a previous paper [5], we described the design of the prototype, XRPIX1, and reported results from it. XRPIX1 has successfully detected hard X-rays in the range from 8 keV to 60 keV with good linearity between energy and pulse height withresponsivity (i.e., output gain) of 3.56 μV/electron. A depletion depth of 150 μm was achieved at a detector bias of 100 V using the Czochralski type wafer. Even deeper full depletion of 260 μm was reported [9] with the high-resistivity (FZ-type) wafer.

The readout noise of XRPIX1 was 120–130 electrons rms [5] in the full-frame readout mode, dominated by the reset noise at the sense node, with some contributions from white and 1/f noises. The high noise level limited further investigations of other parameters of the device. Increasing the gain is a direct way to obtain a higher signal-to-noise ratio.

This paper reports the X-ray results for an improved chip (XRPIX1b) in a frontside illumination configuration. XRPIX1b design was revised to improve the sense-node gain (section II, V). We applied a multiple sampling method described in [4] to further reduce the readout noise (section IV), which allows us to measure the soft X-ray response and the circuitry crosstalk (section V). Relevant results on backside-illuminated SOI pixel sensor with a different implementation (the same basic technology was used) were recently described in [12].

The uncertainties given throughout this paper are statistical only and correspond to the 90% confidence level (1.64 sigma) range unless noted otherwise.

II. Device Description

XRPIX1b was fabricated with 0.2 μm SOI CMOS process by Lapis Semiconductor Ltd. Figure 1 shows the design of the sensor. The format and pixel circuitry are the same as those of XRPIX1. The chip consists of 32 × 32 pixels with a size of 30.6 μm square. Each pixel contains a SOI-CMOS

Manuscript received June 21, 2012; accepted November 25, 2012. This work was supported by the Japan Society for the Promotion of Science (JSPS; KAKENHI 21244040), the Grant-in-Aid for the Global COE Program "The Next Generation of Physics, Spun from Universality and Emergence" from the Ministry of Education, Culture, Sports, Science and Technology (MEXT) of Japan, and the KEK Detector Technology Project. TGT is supported by Scientific Research B (Nos. 20340043 and 23340047). This work is also supported by VLSI Design and Education Center (VDEC), the University of Tokyo in collaboration with Synopsys, Inc., Cadence Design Systems, Inc., and Mentor Graphics, Inc.

S. G. Ryu, T. G. Tsuru, and S. Nakashima are with the Department of Physics, Graduate School of Science, Kyoto University, Sakyo-ku, Kyoto 606-8502, Japan (telephone: +81-75-753-3827, email: ryu@cr.scphys.kyoto-u.ac.jp).

G. Prigozhin, R. F. Foster, S. Kissel, B. LaMarr, and M. Bautz are with Kavli Institute for Astrophysics and Space Research, Massachusetts Institute of Technology, Cambridge, MA 02139 USA.

A. Takeda and Y. Arai are with the Institute of Particle and Nuclear Studies, High Energy Accelerator Research Org., KEK, Tsukuba 305-0801, Japan. A. Takeda is also with the Graduate University for Advanced Studies (SOKENDAI), School of High Energy Accelerator Science.

T. Imamura, T. Ohmoto, and A. Iwata is with A-R-Tec Corp., Saijo Otsubo-cho, Higashi-Hiroshima, Hiroshima 739-0005, Japan.

circuit capable of analog correlated-double-sampling readout and trigger detection (see Fig. 1(b)). Details of the CMOS process and the full circuit operation are described in [5]. The sensor layer used in this work is n-type silicon (Czochralski type) with resistivity of $\rho\sim$ 700 Ω cm. The wafer was the same type as XRPIX1, but manufactured in a different run. It was thinned down to 100 μm from the backside. The back surface of the device after thinning was treated by CMP (chemical mechanical polish) in order to prevent leakage currents when the depletion layer reaches the back surface. The property of the CMP treatment is described in [9].

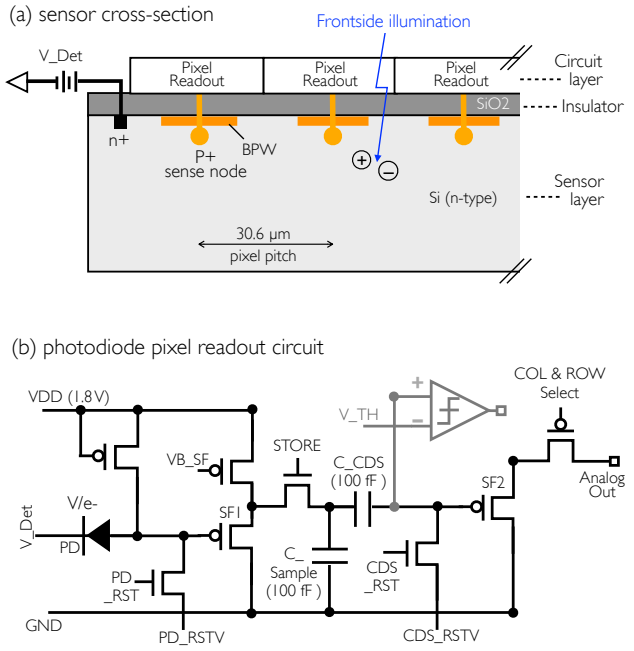

Fig. 1. Design of SOIPIX prototype XRPIX1b. (a) schematic cross-section view (not to scale). BPW represents the buried p-well. (b) readout circuitry of one pixel. The trigger part, which is not operated in this work, is shown in the grey solid lines.

XRPX1b is different from XRPIX1 in size of the buried p+ well (BPW; see Fig. 1(a)). BPW is a lightly p-type doped region surrounding the central sense-node, which is necessary as an electrical shield to suppress the back-gate effect under a high detector bias (see details of this technology in [11]). Results from [5] indicate that the sense-node capacitance of XRPIX1 is mainly due to the BPW-BPW coupling between adjacent pixels. In an attempt to increase the sense-node gain, we reduced the BPW area by 45% from XRPIX1 (21 μm square) to XRPIX1b (14 μm square), which is expected to decrease the capacitance approximately by the same percentage. With a TCD (technology computer aided design) simulation [10], we confirmed that this BPW size is sufficient to keep the transistors functional under a detector bias up to 100 V.

III. Experimental Setup

The XRPIX1b chip was packaged and mounted on a dedicated readout board [11][5]. The experiments were performed in a vacuum chamber in which the chip was cooled to -50°C through a thermal contact between the chip package and liquid

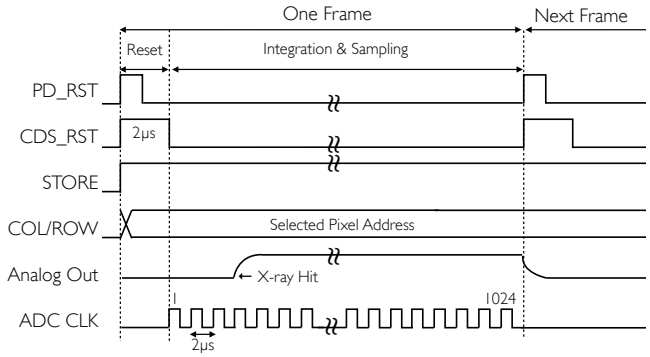

Fig. 2. Timing diagram of the multi-sampling readout mode.

nitrogen. The temperature was the same as the experiments of XRPIX1 reported in [5]. The incident X-rays were generated by an electron impact source with the targets of aluminum (Al) and iron (Fe) under the generator bias of 6 kV and 10 kV, respectively. We also used a CCD [8] to confirm the output spectrum, which contained the characteristic X-rays of the target materials and the bremsstrahlung continuum. Detector bias (V_Det; Fig. 1) of 100V was applied to the XRPIX1b. At this voltage, the sensor layer is expected to be fully depleted with a 100 μm thickness according to the previous results [5]. In this work, the chip was illuminated from the circuit side, or in frontside illumination.

IV. Data Acquisition and Analysis

In order to reduce readout noise, we read out the analog signal from one pixel multiple times, using a technique similar to the one described in [4]. The trigger function was not used in this work. The timing diagram is shown in Fig. 2. Prior to readout, the pixel photodiode is reset (PD_RST and CDS_RST are turned on and off). So-called kT/C noise (or reset noise) is generated in this phase. Reset is followed by an integration time when the pixel awaits an X-ray hit. During integration, the analog output is digitized consecutively 1024 times, and the results are recorded in a computer as a single frame. Time intervals between digital samples are 2 μs (Al data). The digitization is performed by an ADC on the readout board; one analog digital unit (ADU) is 1V/12 bit = 244 μV.

Figure 3 shows a typical waveform for a frame in which an X-ray photon is observed. A clear jump in pulse height (PH) corresponds to the moment when an X-ray photon is detected. The X-ray energy can be measured as the difference between signal levels before and after the jump. One can see noticeable scatter of the signals ($\leq$ 5 ADU) on either side of the X-ray jump. This is caused by the readout noise. Since all the samples within one frame are obtained without resetting the sense node, the kT/C noise should be absent here. Therefore, the readout noise is a superposition of the white noise and the 1/f noise in the transistors, the ADC quantization noise, and external noises from peripheral IC chips on the readout board. The quantitative decomposition of the readout noise can be found in [5]. We also notice a systematic signal level rise with time (see Fig. 3). This is probably due to dark current, which is about $\sim 10^2$ electrons /ms /pixel at -50°C.

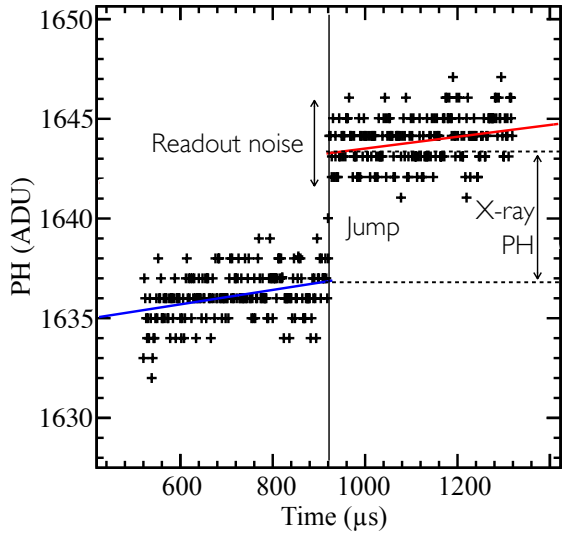

Fig. 3. Waveform of an X-ray event by 400 consecutive samples. The sampling frequency is 500 kHz. One ADU is 244 μV. The best-fit linear function for the data points before and after the X-ray jump is shown in the blue and red solid lines, respectively.

In order to properly estimate the X-ray PH and the readout noise, we apply the following method (one can call it multi-point correlated sampling) to each frame of data:

1) Scan the consecutive data points for a threshold (e.g., 2 sigma of the noise level) to detect the time of the X-ray jump. If no jump is detected, the jump time is assumed to be at the middle of the frame. This is for noise estimation purposes.
2) Fit the data points before and after the jump time with two linear functions (see Fig. 3).
3) Compute the PH as the difference of the signal values before and after the the jump time (Fig.3) from the best-fit parameters of the linear functions.
4) Make a histogram of the resulting PH, which is the spectrum of the incoming X-ray events. The non-X-ray events produce a gaussian peak around zero whose width corresponds to the readout noise.

This method has two merits. Firstly, we can take into account the PH increase due to dark current since we use linear functions to reproduce the slope. Secondly, the fitting process for multiple data points on each side of the jump is equivalent to averaging the PH values, which acts as a low-pass filter reducing the readout noise. We are also able to read out 3×3 pixels and obtain 9 waveforms simultaneously in the same way as described above. The sampling frequency (data points) for each waveform is more limited because we use one ADC to convert the analog signals of 9 pixels sequentially instead of focusing on one pixel.

V. Experiment Results

A. Soft X-ray Response and Gain

Figure 4 shows X-ray spectra obtained from a single pixel with Al and Fe targets. The sampling frequency for each data point in the waveform is 500 kHz. The characteristic X-ray lines of Al Kα (1.49 keV), Fe Kα (6.4 keV), and Fe Kβ (7.0 keV) are well resolved. In the Fe spectra (Fig.4(b)), the silicon-absorption edge at 1.8 keV due to the frontside circuit layer is observed. The low-energy shoulder at ∼0.7 keV is probably due to partial charge collection. The high-energy tails above the main peaks (e.g., 2–5 keV in Fig. 4(a)) are from bremsstrahlung by impact electrons.

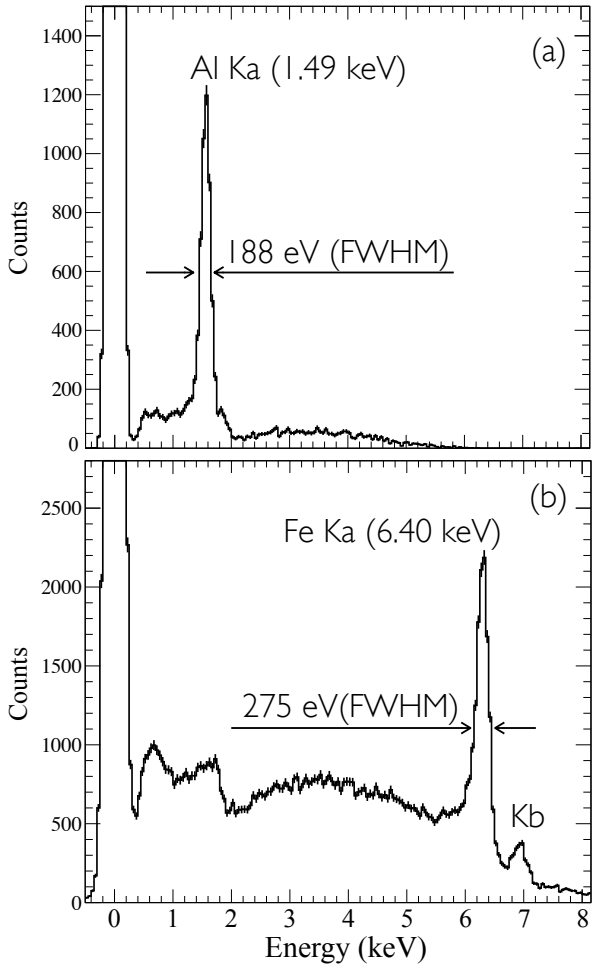

Fig. 4. X-ray spectra of the Al (a) and Fe (b) primary sources with the chip in frontside illumination. Each spectra has an exposure of 400 s.

The energy (keV) - PH (ADU) dependence (Fig. 5) shows good linearity in soft X-ray regime. The output gain (responsivity) is calibrated to be 6.0 μV/electron (best-fit value), which is an improvement over the previous chip (XRPIX1) by a factor of 1.7. Since the gain is inversely proportional to the sense-node capacitance, this improvement is roughly consistent with the expectation from the smaller capacitance by cutting half of the BPW area (c.f., section-II; [5]).

The energy resolution (full width at half maximum; FWHM) is 188±5 eV at 1.49 keV (Al Kα) and 275±10 eV at 6.40 keV (Fe Kα). The readout noise of the Al and Fe data are 18 and 22 electrons rms, respectively. The observed FWHM of the Al line is close to the prediction from the readout noise and the fano noise, i.e., $\sqrt{18^2 + (1490/3.65 \times 0.12)} \times 2.35 \times$ 3.65 eV/electron = 166 eV, assuming a fano factor of 0.12 in silicon. The difference between the prediction and the

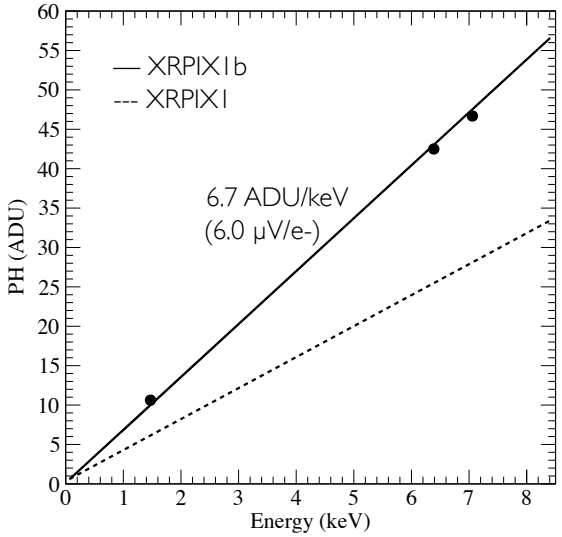

Fig. 5. Energy calibration of XRPIX1b with the observed X-ray pulse height (PH) and the corresponding energies. Data points and the best-fit model (linear function) are shown with the filled circles and the solid line, respectively. For comparison, the result of XRPIX1 [5] is shown in the dashed line.

measurement could be due to charge collection inefficiency although this is still under investigation.

The readout noise (∼20 electrons rms) is substantially improved over previous work (129 electrons rms; [5]) by a factor of ∼6. This improvementis comprised of the increase of the gain (factor of ∼2) and the effect of multi-point correlated sampling (factor of ∼3). Still, the energy resolution is effectively limited by the readout noise. Following is a strategy to achieve the fano limit (<10 electrons). According to TCAD simulations [10], we can further reduce the BPW area by ∼50% (14 to 10 μm square) to increase the gain (i.e., signal/noise ratio) without serious back-gate effects. An optimization of the low-pass filter to reduce white noises (section IV) is necessary. A Δ-Σ ADC for reduction of white noise using the same SOI process is described in [13].

B. Circuitry Crosstalk

In order to measure the circuitry crosstalk between adjacent pixels, we followed the approach described in [4]. We use 6.4 keV X-rays (Fe Kα) as input signals. We acquire data from 3×3 pixel island in a multi-sample method similar to our single pixel multi-sample readout (section IV). The sampling frequency for each data point in the waveform is 110 kHz. The readout noise is 48 electrons rms.

We first check the non-uniformity of the distribution of the 6.4 keV line centers (ADU) in all of the tested 3×3 pixels. The gain dispersion is measured to be 0.8 % (standard deviation). The non-uniformity is consistent with the result of XRPIX1 [9] and is 2–3 times smaller in comparison with the other APSs (e.g., [2]).

Single-pixel events are selected in the following way. We focus on the center pixel and select the events whose PH is located in the right half of the 6.4 keV gaussian at 3 sigma level (6.4–6.9 keV). These events should have the holes produced by one 6.4 keV photon fully collected in the center pixel (see [4] for more explanation). We plot averaged waveforms for the 3×3 pixels to investigate the crosstalk. As shown in Fig. 6, no substantial PH variance in the adjacent pixels is observed at the moment when the center pixel detects a 6.4 keV photon, which suggests small crosstalk between the adjacent pixels.

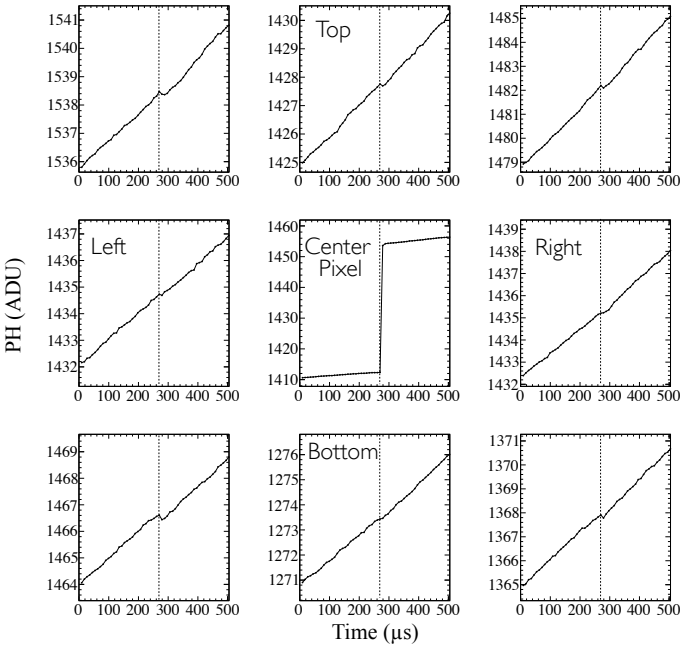

Fig. 6. Averaged waveform of 3×3 pixels for the single-pixel 6.4 keV X-ray events. The vertical dashed lines in each panel indicated the time when an X-ray photon is detected in the center pixel.

For more quantitative estimation, we compute changes in PH of the surrounding 8 pixels at the time of a X-ray jump in the center pixel in the same way as we calculate the X-ray PH of a single pixel (see section IV). The results are shown in Fig.7. The positions of the PH peaks (best-fit value with gaussian function) around zero are equivalent to the crosstalk. The crosstalk in adjacent pixels is in the range 0.2–0.5%, in the opposite direction with respect to the signal at the center pixel. It can be seen as a small dip in the middle of each graph in Fig.6.

Usually crosstalk is problematic when reconstructing PH, i.e., adding signals from adjacent pixels [9] for charge splitting events (section V-C). In the case of XRPIX1b, the measured crosstalk of the 6.4 keV signal corresponds to 0.1–0.25 ADU or 4–10 electrons (holes), which is negligible at the present noise level. It is worth noting that the observed crosstalk is quite small compared with other APSs (e.g., [4]).

C. Charge Splitting Event

A charge splitting event occurs if holes produced by an X-ray photon are collected by more than one pixel. The center pixel containing the largest amount of charge has the highest PH among the adjacent pixels. In general, probability of charge splitting depends on the pixel size, the charge-cloud size when it reaches the sense node, and the location of the photon interaction in the pixel.

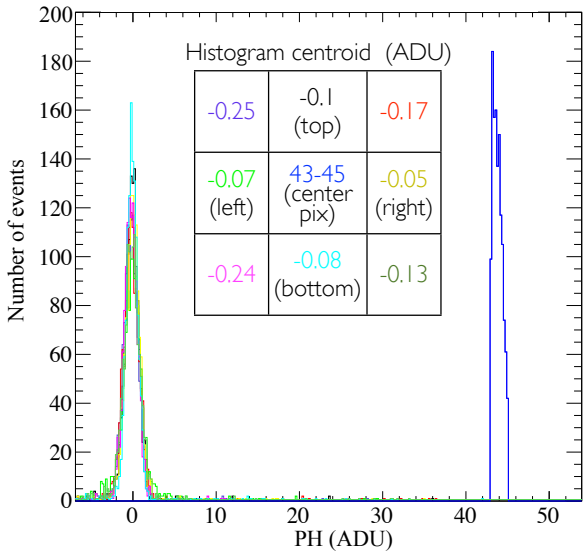

Fig. 7. PH histograms of the center pixel and adjacent pixels for the extracted single-pixel events of the 6.4 keV X-ray (see text in section V-B). The best-fit histogram centroid (ADU) of adjacent pixels, shown in the embedded table, corresponds to the crosstalk. Results of different pixels are shown in different colors.

Using the 3×3 pixel data with the Al and Fe targets, we measure fractions of each event type: single-pixel, double-pixel, and the other multi-pixel events for each X-ray energy. The event selection (c.f., [5]) is performed with an event threshold of 4 sigma and a split threshold of 2 sigma significance with respect to the noise level (48 electrons rms). According to the results in section III-B, the effect of crosstalk is negligible in this measurement. The results are shown in table I.

TABLE I
CHARGE SPLITTING EVENT RATIO

Event type	Event ratio (Al, 1.5 keV)	Event ratio (Fe, 6.4 keV)
Single pixel	87.4 ± 1.6%	80.6± 1.2%
Doule pixel	7.4 ± 0.3%	13.4± 0.4%
Others	5.2 ± 0.3%	6.0 ± 0.3%

We found that most X-ray events are confined to one pixel rather than split between multiple pixels; the single-pixel event fractions are 87% and 80% for the Al and the Fe data, respectively. This is not surprising considering the small size of the initial charge cloud (100–300 nm at these energies; e.g., [14]) relative to the pixel size of 30 μm. The Fe (6.4 keV) data contain more charge splitting events than the Al (1.5 keV) data. The X-rays with higher energy are absorbed deeper in the silicon bulk due to longer attenuation length in silicon, and because of thermal diffusion that results in larger charge cloud size when reaching the sense node.

With a thicker depletion layer (>100 μm) or in backside illumination, more multi-pixel events are expected because more photons are absorbed near the back surface, i.e., far from the sense node. Enlarging the pixel size is a direct way to achieve a high single-pixel fraction. According to results shown in table I, a double-size pixel, which is manufacturable, should have single-pixel fraction of ∼95% at 6 keV.

VI. CONCLUSIONS

We investigated the characterizations of a revised SOIPIX chip (XRPIX1b) in the frontside illuminated configuration using X-rays from 1.49 to 7.0 keV. We found that the responsivity is improved to 6 μV/electron. The energy resolution is 188 eV (FWHM) at 1.5 keV, in a readout noise of 18 electron rms. The gain non-uniformity among pixels is 0.8 % (standard deviation). The circuit crosstalk in adjacent pixels is less than 0.5 %. More than 80% of the X-ray events are those collected in one pixel.

ACKNOWLEDGMENT

We are grateful to all members of the SOI group, especially Y. Ono for the TCAD simulations. We appreciate M. Okihara and H. Kasai from Lapis for providing the information on the SOI process. We also thank T. Tanaka for improving the draft quality.

REFERENCES

[1] N. Wermes et al."New Results on DEPFET Pixel Detectors for Radiation Imaging and High Energy Particle Detection", *IEEE Trans. Nucl. Sci.*, vol.51, no.3, pp.1121-1128, 2004.
[2] L. Bombelli et al."First Readout of a 64 × 64 DEPFET Matrix With VELA Circuit", *IEEE Trans. Nucl. Sci.*, vol.56, no.6, pp.3789-3795, 2009.
[3] P. Lechner et al., "The IXO Wide-Field Imager", in *Proc. SPIE*, Vol. 7742, 77420T-8, 2010.
[4] G. Prigozhin et al., "Characterization of Three- Dimensional-Integrated Active Pixel Sensor for X-Ray Detection", *IEEE Trans. Nucl. Sci.*, vol.56, no.11, pp.2602-2611, 2009.
[5] S. G. Ryu et al., "First Performance Evaluation of an X-Ray SOI Pixel Sensor for Imaging Spectroscopy and Intra-Pixel Trigger", *IEEE Trans. Nucl. Sci.*, vol.58, no.5, pp.2528-2536, 2011.
[6] G. P. Garmire, M. W. Bautz, P. G. Ford, J. A. Nousek, and G. R. Jr. Ricker, "Advanced CCD imaging spectrometer (ACIS) instrument on the Chandra X-ray Observatory", in *Proc. SPIE*, Vol. 4851, pp. 28-44, 2003.
[7] L. Strüder et al., "The European Photon Imaging Camera on XMM-Newton: The pn-CCD camera", *Astronomy & Astrophysics*, 365, L18, 2001.
[8] K. Koyama et al., "X-Ray Imaging Spectrometer (XIS) on Board Suzaku", *Publications of the Astronomical Society of Japan*, 59, S23-33, 2007.
[9] S. Nakashima et al., "Progress in Development of Monolithic Active Pixel Detector for X-ray Astronomy with SOI CMOS Technology", *Physics Procedia*, vol. 37C, pp. 1392-1399, DOI: 10.1016/j.phpro.2012.04.100, 2012
[10] SOIPIX Collaboration. http://rd.kek.jp/project/soi/ .
[11] Y. Arai, et al., "Development of SOI pixel process technology", *Nucl. Instrum. Methods*, Volume 636, Issue 1, Supplement 1, Pages S31-S36, 2011.
[12] M. Battaglia et al., "Characterisation of a Thin Fully Depleted SOI Pixel Sensor with Soft X-ray Radiation", *Nucl. Instrum. Methods*, doi:10.1016/j.nima.2012.01.054
[13] S. Nakashima et al., "Development of a built-in analog-to-digital converter for a X-ray astronomy detector with the SOI CMOS technology", in Proc. *IEEE Nuclear Science Symp. Conf.*, pp. 1201-1203, 2011.
[14] G. Prigozhin et al., "The physics of the low-energy tail in the ACIS CCD The spectral redistribution function", *Nucl. Instrum. Methods*, Volume 439, Pages 582-591, 2000.